Giacometti, G. M., Brunori, M., Antonini, E., Dilorio, E. E., & Winterhalter, K. H. (1980) *J. Biol. Chem. 255*, 6160-6165.
Gibson, Q. H., Parkhurst, L. J., & Geraci, G. (1969) *J. Biol. Chem. 244*, 4668-4676.
Golding, R. M., Singhasowich, T., & Tennant, W. C. (1977) *Mol. Phys. 34*, 1343-1350.
Griffith, J. S. (1956) *Proc. R. Soc. London, A 235*, 23-36.
Hayashi, A., Suzuki, T., Shimizu, A., Morimoto, H., & Watari, H. (1967) *Biochem. Biophys. Acta 147*, 407-409.
Higuchi, Y., Kusunoki, M., Matsuura, Y., Yasuoka, N., & Kakudo, M. (1984) *J. Mol. Biol. 172*, 109-139.
Iizuka, T., & Kotani, M. (1969) *Biochem. Biophys. Acta 194*, 351-363.
Keller, H., & Debrunner, P. G. (1980) *Phys. Rev. Lett. 45*, 68-71.
Levy, A., & Rifkind, J. M. (1985) *Biochemistry 24*, 6050-6054.
Levy, A., Walker, J. C., & Rifkind, J. M. (1982) *J. Appl. Phys. 53*, 2066-2068.
Levy, A., Alston, K., & Rifkind, J. M. (1984) *J. Biomol. Dyn. 1*, 1299-1309.
Mayo, K. H., Kucheida, D., Parak, F., & Chien, J. C. W. (1983) *Proc. Natl. Acad. Sci. U.S.A. 80*, 5294-5296.
Mims, M. P., Porras, A. L., Olson, J. S., Noble, R. N., & Peterson, J. P. (1983) *J. Biol. Chem. 258*, 14219-14232.
Palmer, G. (1985) *Biochem. Soc. Trans. 13*, 548-560.
Papaefhtymiou, G. C., Huynh, B. H., Yens, C. S., Groves, J. L., & Wu, C. S., (1975) *J. Chem. Phys. 62*, 2995-3001.
Peisach, J., Blumberg, W. E., Wittenberg, B. A., Wittenberg, J. B., & Kampa, L. (1969) *Proc. Natl. Acad. Sci. U.S.A. 63*, 934-939.
Peisach, J., Blumberg, W. E., Ogawa, S., Rachmilewitz, E. A., & Oltzik, R. (1971) *J. Biol. Chem. 246*, 3342-3355.
Peisach, J., Blumberg, W. E., & Adler, A. (1973) *Ann. N.Y. Acad. Sci. 206*, 310-327.
Rein, H., Ristau, O., Janig, G. R., & Jung, F. (1971) *FEBS Lett. 15*, 21-23.
Rifkind, J. M. (1979) *Biochemistry 18*, 3860-3865.
Rifkind, J. M. (1988) in *Heme Proteins* (Eichhorn, G. L., & Marzilli, L. G., Eds.) Advances in Inorganic Biochmistry 7, pp 155-245, Elsevier, New York.
Shaanan, B. (1983) *J. Mol. Biol. 171*, 31-59.
Tucker, P. W., Phillips, S. E. V., Perutz, M. F., Houtchens, R., & Caughey, W. S. (1978) *Proc. Natl. Acad. Sci. U.S.A. 75*, 1076-1080.
Yamamoto, Y., & LaMar, G. N. (1986) *Biochemistry 25*, 5288-5297.
Yonetani, T., Iizuka, T., & Waterman, M. R. (1971) *J. Biol. Chem. 246*, 7683-7689.

Small-Angle Scattering Studies Show Distinct Conformations of Calmodulin in Its Complexes with Two Peptides Based on the Regulatory Domain of the Catalytic Subunit of Phosphorylase Kinase†

J. Trewhella,*,‡ D. K. Blumenthal,§ S. E. Rokop,‡ and P. A. Seeger‡

Life Sciences and Physics Divisions, Los Alamos National Laboratory, Los Alamos, New Mexico 87545, and Department of Biochemistry, University of Texas Health Center at Tyler, Tyler, Texas 75710

Received March 30, 1990; Revised Manuscript Received June 14, 1990

ABSTRACT: Small-angle X-ray and neutron scattering have been used to study the solution structures of calmodulin complexed with synthetic peptides corresponding to residues 342-366 and 301-326, designated PhK5 and PhK13, respectively, in the regulatory domain of the catalytic subunit of skeletal muscle phosphorylase kinase. The scattering data show that binding of PhK5 to calmodulin induces a dramatic contraction of calmodulin, similar to that previously observed when calmodulin is complexed with the calmodulin-binding domain peptide from rabbit skeletal muscle myosin light chain kinase. In contrast, calmodulin remains extended upon binding PhK13. In the presence of both peptides, calmodulin also remains extended. Apparently, the presence of PhK13 inhibits calmodulin from undergoing the PhK5-induced contraction. These data indicate that there is a fundamentally different type of calmodulin–target enzyme interaction in the case of the catalytic subunit of phosphorylase kinase compared with that for myosin light chain kinase.

Calmodulin is an intracellular Ca^{2+}-binding protein involved in a large number of Ca^{2+}-dependent processes. Structural data on calmodulin and its complexes with its many target enzymes are critical for understanding the molecular basis for how each target enzyme is regulated. The three-dimensional crystal structure of calmodulin has been determined (Babu et al., 1985) and was recently refined to 2.2-Å resolution (Babu et al., 1988). The crystallographic data show many important structural details thought to be important for target enzyme interactions including an eight-turn solvent-exposed α-helix connecting two globular lobes, with each lobe containing two Ca^{2+}-binding domains and a solvent-exposed hydrophobic patch. Although this structure is of high resolution, it may not accurately reflect the structure of the protein when in solution, which is most relevant to questions concerning target enzymic interactions. Indeed, CD[1] studies indicate there is

† This work was performed under the auspices of the DOE (Contract W-7405-ENG-36) and was supported by NIH Grants GM40528 (J.T.), GM39290 (D.K.B.), DOE Project KP-04-01-00-0 (J.T.), and a Grant-In-Aid from the American Heart Association (D.K.B). This work has benefited from the use of facilities at the Manuel Lujan, Jr., Neutron Scattering Center, a national user facility funded as such by the DOE/Office of Basic Energy Sciences.

* Address correspondence to this author at the Life Sciences Division, Los Alamos National Laboratory.
‡ Los Alamos National Laboratory.
§ University of Texas.

0006-2960/90/0429-9316$02.50/0

significantly less α-helix in $4Ca^{2+}$–calmodulin in solution compared with the crystal structure (Bayley et al., 1988).

Small-angle X-ray and neutron scattering techniques can provide information on the overall shapes of proteins in solution. Neutron scattering has the additional advantage that it can provide structural information about individual components of a complex by using deuterium labeling and capitalizing on the different neutron scattering properties of deuterium and hydrogen. In the first X-ray scattering experiments from this laboratory (Heidorn & Trewhella, 1988) it was proposed that the interconnecting helix of calmodulin is flexible in solution and that on average the two globular lobes are closer together than is observed in the crystal form. More recent experiments have focused on X-ray and neutron scattering studies of calmodulin–peptide complexes using synthetic peptides based on calmodulin-binding domains from target enzymes. These peptides are useful models for studying calmodulin–target enzyme interactions [reviewed by Blumenthal and Krebs (1988)], particularly when large quantities of material are required, as is the case for X-ray and neutron scattering experiments. The results of recent X-ray and neutron scattering studies involving a 27-residue synthetic peptide, termed MLCK-I, based on the calmodulin-binding domain of rabbit skeletal muscle myosin light chain kinase indicate that MLCK-I causes a dramatic contraction of calmodulin's structure, which brings the two lobes of calmodulin into close contact (Heidorn et al., 1989).

Phosphorylase kinase is an unusual calmodulin-dependent enzyme in that calmodulin is an integral subunit (termed the δ-subunit) which does not readily dissociate from the holoenzyme when Ca^{2+} concentrations are lowered to submicromolar levels (Picton et al., 1980). The Ca^{2+}-dependent catalytic activity of phosphorylase kinase is thought to be regulated by direct interactions between the δ-subunit and the catalytic subunit [termed the γ-subunit; reviewed by Pickett-Giess and Walsh (1986)]. Whereas most calmodulin target enzymes have calmodulin-binding domains that span less than 30 residues, the γ-subunit calmodulin-binding domain spans approximately 70 residues and is divided into two noncontiguous subdomains that interact with calmodulin simultaneously (Dasgupta et al., 1989). Synthetic peptides, 25 residues in length, corresponding to each of the two subdomains have been prepared to characterize their respective individual and combined interactions with calmodulin by using X-ray and neutron scattering. Solution structural data for these γ-subunit peptide–calmodulin complexes are presented here and are compared to previously characterized structures of calmodulin and calmodulin–peptide complexes.

Materials and Methods

Sample Preparation. The two peptides, designated PhK5 and PhK13, were chemically synthesized with the following sequences: LRRLIDAYAFRIYGHWVKKGQQQNRG-amide (PhK5); and RGKFKVICLTVLASVRIYYQYR-RVKPG-amide (PhK13). The methods of synthesis and purification are detailed in Dasgupta et al. (1989).

Deuterated calmodulin was produced by using a bacterial expression system as described in Heidorn et al. (1989), except that the deuterated algal hydrolysate was derived from a mixture of deuterated algae that was approximately 50% *Chlorella vulgaris*, 20% *Phormidium luridum*, 20% *Anacystis nidulans*, and 10% *Synechococcus lividus*. The amino acid composition of the hydrolysate was determined by amino acid analysis. The hydrolystate was then diluted with nondeuterated amino acids such that the ratio of deuterated to nondeuterated amino acids was approximately 3:1. In addition, the growth medium was made up with 75% D_2O. This strategy was used to obtain calmodulin that was partially deuterated.

Samples of calmodulin complexed with each peptide were prepared with 1:1 stoichiometries by using concentration values for the constituents based on measured optical densities at 277 nm and assuming extinction coefficients of $\epsilon^{0.1\%} = 0.18$ for calmodulin (Watterson et al., 1976) and $\epsilon^{1mM} = 8.1$ and 3.9 for PhK5 and PhK13, respectively. The extinction coefficients for PhK5 and PhK13 are based on the sum of the extinction coefficients of the Tyr and Trp residues in each peptide (Fasman, 1989). After X-ray and/or neutron measurements were completed, protein/peptide concentrations were determined more precisely by quantitative amino acid analysis using a Beckman 6300 analyzer. Histograms of the expected amino acid compositions (assuming 1:1 protein:peptide stoichiometries and using alanine as an internal standard) showed good agreement with the observed amino acid compositions, except for glycine, which was anomalously high due to contamination of one of the hydrolysis reagents by extraneous glycine. All samples of calmodulin and calmodulin–peptide complexes were made up in buffered solutions containing 100 mM KCl and 50 mM Tris-HCl, pH 7.4, with 20 mM $CaCl_2$.

Scattering Data Acquisition and Analysis. The neutron scattering data were measured by using the low-Q diffractometer (LQD) at the Manuel Lujan, Jr., Neutron Scattering Center, Los Alamos National Laboratory (Seeger et al., 1987, 1990). X-ray scattering data were measured by using the small-angle station at Los Alamos, which is described in detail in Heidorn and Trewhella (1988). For the X-ray measurements reported here the sample-to-detector distance was 63.5 cm. The data acquisition, reduction, and analysis are described in detail in Heidorn et al. (1989) and the references cited therein. Both the Guinier (Guinier, 1939) and indirect Fourier transform [or $P(r)$] data analysis methods gave the same results for the structural parameters determined, within the limits of the uncertainties in the data, and the parameters derived by using both approaches are presented for comparison.

The intensity of scattered neutrons, or X-rays, is measured as a function of scattering angle, $I(\theta)$, and then converted to $I(Q)$, where Q is the amplitude of the scattering vector and is equal to $(4\pi \sin \theta)/\lambda$; θ is half the scattering angle and λ the wavelength of the scattered radiation. Scattering data were analyzed by using the indirect Fourier transform analysis as parameterized by Moore (1980). The functions $QI(Q)$ and $P(r)/r$, where $P(r)$ is the distribution of vector lengths, r, in the scattering particle, are a Fourier transform pair. The model consists of setting $P(r)/r$ equal to zero when $r = 0$, and when r is greater than a maximum vector length d_{max}, then representing it as a series of truncated sine functions between $r = 0$ and $r = d_{max}$. These truncated sine functions transform to a set of basis functions in reciprocal space [in which the scattering data, $I(Q)$, are collected]. The parameter d_{max} derived from small-angle scattering data should always be treated with some caution since there is no good a priori way for determining d_{max}. For the current analysis, Moore's pro-

[1] Abbreviations: CD, circular dichroism; d_{max}, maximum linear dimension; $\epsilon^{0.1\%}$, extinction coefficient for a 1 mg/mL solution; ϵ^{1mM}, extinction coefficient for a 1 mM solution; MLCK, myosin light chain kinase; MLCK-I, 27-residue synthetic peptide corresponding to residues 577–603 of rabbit skeletal myosin light chain kinase; NMR, nuclear magnetic resonance; PhK5 and PhK13, 25-residue synthetic peptides corresponding to residues 342-366 and 301–326, respectively, of the catalytic subunit of rabbit skeletal phosphorylase kinase; R_g, radius of gyration; R_v, radius of gyration at infinite contrast; Tris, tris(hydroxymethyl)aminomethane.

cedure (Moore, 1980) was used; i.e., d_{max} was chosen as the minimum value which gives a good fit to the data and also keeps $P(r)$ positive at $r < d_{max}$. For the two more extended complexes (calmodulin + PhK13 and calmodulin + PhK5 + PhK13) the accuracy of the determination of d_{max} is somewhat problematic due to the lack of quality data below $Q = 0.02$ Å, which is influential in determining such large values of d_{max} (Moore, 1980). This was not the case for the more compact calmodulin and calmodulin + PhK5 complex, which have much smaller d_{max} values. The R_g value for a particle can be calculated from the second moment of its model $P(r)$, and comparison of this R_g value with that determined from the Guinier analysis provides a good check for the accuracy of the model. The values for radius of gyration, R_g, used in the discussion of the results are from the $P(r)$ analysis since this analysis uses more of the scattering data and therefore generally has higher statistical precision. Radius of gyration is the root-mean-square weighted distance of all elemental scattering volumes from the center of scattering density and is analogous to the spherically averaged moment of inertia for a rigid body.

The number of sine terms, n, that can be determined in the $P(r)$ series expansion is limited by $d_{max}Q_{max}/\pi$, where Q_{max} is the maximum scattering vector for which data are obtained in the experiment; this truncation in data space can lead to artifacts, such as ripples, in the transform. If Q_{max} is large enough to be in the Porod region (Porod, 1951) so that $I(Q)$ may be assumed to extrapolate as Q^{-4} for $Q > Q_{max}$, then coefficients of additional terms would obey a simple numerical relationship. Specifically, the last basis function may be modified by including the appropriate linear combination of the next two orders. This assumption was not used in the analysis of the neutron scattering data for calmodulin + MLCK-I (Heidorn et al., 1989), because these data did not always extend to a region where the Q^{-4} proportionality could be established. For larger particles (like calmodulin + PhK5 + PhK13), however, the Porod region occurs at lower Q values. The present neutron and X-ray data were analyzed both with and without the Q^{-4} assumption, and no significant differences were found in the respective R_g, d_{max}, or $I(0)$ values. When the modified basis function is used with these data, the transformation is less susceptible to the introduction of unrealistic high-order ripples in the $P(r)$ curves. For this reason, the $P(r)$ curves presented in this paper are those obtained from the analysis that included the Q^{-4} assumption.

X-ray data were measured from 0.02 to 0.3 Å^{-1}. For the Guinier analyses, only data for which $QR_g < 1.3$ (where the Guinier approximation can be assumed to be valid) were used. The $P(r)$ analyses for calmodulin alone and for calmodulin + PhK5 are quite insensitive to the exact data range analyzed, but the data for calmodulin + PhK13 and calmodulin + PhK5 + PhK13 (which have significantly larger R_g values and hence a narrower Guinier region than the former) give R_g values that vary somewhat, depending on the exact Q range used in the analysis. For these latter complexes there is increased uncertainty, therefore, in the absolute d_{max} and R_g values determined from the $P(r)$ analysis. The structural parameters given in the tables correspond to those obtained by using a Q range for which the value of R_gQ_{max} was constant (approximately 3.7). For this data range there was good agreement between the R_g values derived from the Guinier and $P(r)$ analyses. Including data with larger Q values for the $P(r)$ analysis resulted in larger R_g values by approximately 1–2 Å.

Neutron data were measured by using partially deuterated calmodulin complexed with nondeuterated PhK5 and PhK13

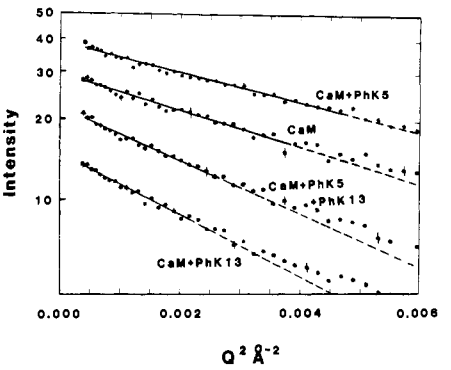

FIGURE 1: Guinier plots for calmodulin + PhK5 (13.3 mg/mL), calmodulin (18.3 mg/mL), calmodulin + PhK5 + PhK13 (9.9 mg/mL), and calmodulin + PhK13 (12.8 mg/mL). The concentrations given as milligrams per milliliter refer to the protein plus peptide concentrations. The intensities are in arbitrary units, and the lower three plots are offset on the intensity scale to avoid overlaps. The solid lines are the Guinier fits to the data, while the dotted lines are the extrapolations of these fits. Representative errors based on counting statistics are shown.

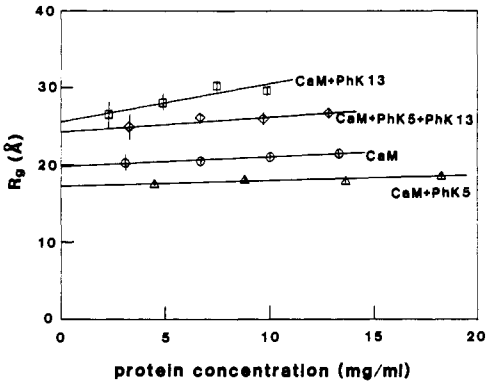

FIGURE 2: Concentration dependence of R_g determined from the X-ray scattering data by using the $P(r)$ analysis for calmodulin (○), calmodulin + PhK5 (△), calmodulin + PhK13 (□), and calmodulin + PhK5 + PhK13 (◇).

with four different solvent contrasts (0%, 20%, 40%, and 100% D_2O) to obtain information about the individual components in the complex. The higher Q neutron data are statistically poorer than the X-ray data, due to incoherent scattering from hydrogen in the samples. Therefore, only the derived parameters R_g and $I(0)$ are reported for the neutron data.

RESULTS

X-ray Scattering. Data were collected for samples of calmodulin and calmodulin complexed with equimolar amounts of PhK5, PhK13, and PhK5 + PhK13, each at four protein concentrations in the range 5–20 mg/mL. The calcium ion concentration (20 mM) was sufficient to saturate the four calcium binding sites in calmodulin for all samples. Figure 1 shows sample Guinier plots for each complex. The differences in slope of the Guinier plots for each complex due to the differences in their R_g values are evident. Figure 2 and Table I show the concentration dependence of structural parameters determined from the $P(r)$ and Guinier analyses of the X-ray scattering data. The errors indicated are the propagated statistical standard deviations only. The R_g and $I(0)$ values determined by using the $P(r)$ analysis agree well with those derived from Guinier analysis for each sample. In most cases, for both $P(r)$ and Guinier analyses, the reduced χ^2 of the fit (given in Table I) is within 1 standard deviation of its expectation value, which is a function of the number of degrees of freedom; the worst case is calmodulin + PhK5 at 4.5 mg/mL protein concentration for which the $P(r)$ χ^2 is 2

Table I: X-ray Scattering Results for Calmodulin with the PhK5 and PhK13 Peptides

		$P(r)$ analysis			Guinier analysis	
	concn (mg/mL)	R_g (Å)	χ^2	n^a	R_g (Å)	χ^2
calmodulin	13.3	21.5 ± 0.36	1.1	4	21.6 ± 0.4	1.3
	10.0	21.1 ± 0.34	1.0	4	21.0 ± 0.4	0.9
	6.7	20.5 ± 0.46	1.1	4	20.3 ± 0.5	0.5
	3.1	20.4 ± 1.10	1.1	4	19.2 ± 1.1	1.3
calmodulin + PhK5	18.3	18.8 ± 0.13	1.2	3	19.6 ± 0.2	1.1
	13.7	18.2 ± 0.16	0.9	3	18.4 ± 0.3	0.7
	8.8	18.1 ± 0.19	1.1	3	17.6 ± 0.4	1.1
	4.5	17.7 ± 0.23	1.3	3	17.9 ± 0.7	0.9
calmodulin + PhK13	9.9	29.7 ± 0.6	1.0	4	28.3 ± 0.5	1.0
	7.5	30.5 ± 0.8	0.6	4	28.5 ± 0.6	0.7
	4.9	28.4 ± 1.1	0.9	4	26.6 ± 0.8	1.1
	2.3	26.5 ± 1.7	0.8	4	24.9 ± 1.2	1.0
calmodulin + PhK5 + PhK13	12.8	26.9 ± 0.6	0.9	4	25.9 ± 0.6	0.8
	9.7	26.0 ± 0.8	1.0	4	24.9 ± 0.6	1.4
	6.7	26.2 ± 0.5	1.1	3	22.8 ± 0.8	1.4
	3.3	24.9 ± 1.6	1.1	4	23.9 ± 1.2	1.2

[a] n is the number of sine terms in the $P(r)$ series expansion (see Materials and Methods).

Table II: Structural Parameters for Calmodulin with PhK5 and PhK13 Calculated by Extrapolation of X-ray Data to Infinite Dilution

	R_g (Å)	d_{max} (Å)	$I(0)/c^a$	obsd ratio[b]	expected ratio[b]
calmodulin	19.9 ± 0.19	66	190 ± 5	1.0 ± 0.05	1.0
calmodulin + PhK5	17.3 ± 0.19	49	206 ± 8	1.1 ± 0.1	1.2
calmodulin + PhK13	25.8 ± 1.4	84	294 ± 22	1.5 ± 0.2	1.2
calmodulin + PhK5 + PhK13	24.3 ± 0.6	84	224 ± 10	1.2 ± 0.1	1.4

[a] $I(0)/c$ values are given in arbitrary units. [b] The observed ratio is the ratio of $I(0)/c$ for each sample to $I(0)/c$ for calmodulin; the expected ratio is the ratio of the molecular weights for each sample assuming 1:1 stoichiometries for each component in each sample. The errors indicated are the propagated statistical errors and do not account for any uncertainties in protein concentration, c.

standard deviations from the expectation value. For calmodulin, calmodulin + PhK5, and calmodulin + PhK5 + PhK13 there was a very slight positive trend in the plots of R_g vs protein concentration, but in each case the differences in R_g values determined for the highest and lowest concentrations were not significantly different from each other. The calmodulin + PhK13 complex R_g data show a linear dependence with a small positive slope of 0.47 ± 0.18 Å/(mg/mL). Such an increase in R_g as a function of protein concentration is sometimes indicative of a small degree of protein aggregation in the sample, though it can also be attributed to interparticle interference effects arising from weak interactions between the particles (Wu & Chen, 1988). Table II gives the R_g values for each complex calculated by extrapolating plots of R_g^2 to infinite dilution according to the method of Zaccai and Jacrot (1983).

For the solution conditions used, previous experiments from our laboratory (Heidorn & Trewhella, 1988) confirm that calmodulin is monodisperse in solution. For the present data, plots of $I(0)/c$ versus c (where c is the protein concentration) are linear, as expected for monodisperse solutions. The extrapolated values of $I(0)/c$ at infinite dilution are also given in Table II, as well as the observed and expected ratios of $I(0)/c$ for each complex to $I(0)/c$ for calmodulin alone. For monodisperse solutions, these ratios are expected to be equal to the respective ratios of the molecular weights of each complex to the molecular weight of calmodulin (Kringbaum & Kugler, 1970). The agreement between the observed and expected ratios is quite good for each sample given the statistical error in $I(0)$ and the error in determining the protein concentration. The $I(0)$ data, therefore, indicate that each of the solutions contained monodisperse particles with relative molecular weights appropriate for each of the calmodulin–peptide complexes. Finally, there is no evidence for upward curvature in the Guinier plots for any of the complexes (Figure 1), also consistent with there being no significant protein aggregation.

The R_g value determined for the partially deuterated calmodulin at zero protein concentration (19.9 ± 0.19 Å) is slightly smaller than the previously determined value of 21.3 ± 0.4 Å for deuterated calmodulin (Heidorn et al., 1989). This difference is within the expected variability between the two different experimental systems. The variability may be mostly attributed to difficulties associated with purifying large quantities (tens of milligrams) of deuterated protein from a bacterial expression system. In previous scattering measurements of deuterated and nondeuterated calmodulin that were prepared by using the same bacterial expression system, we found differences in R_g of about 1 Å between independent preparations [Table I from Heidorn et al. (1989)]. In addition, the current experiments were done by using different solution conditions (20 mM $CaCl_2$ compared with 50 mM $CaCl_2$ used earlier), and there were instrumental differences (the current data were collected by using a longer flight path than was used previously). All of these factors could contribute to the small differences in the measured R_g values. Precautions were taken in the present work to facilitate reliable comparison of the results for each calmodulin complex. All measurements (X-ray and neutron) were done by using partially deuterated calmodulin isolated and purified from the same batch. In addition, all the X-ray measurements were completed with the identical instrument geometry and with the samples in the same capillary.

Figure 3 shows $P(r)$ curves for calmodulin, calmodulin + PhK5, calmodulin + PhK13, and calmodulin + PhK5 + PhK13. The calmodulin $P(r)$ curve is very similar to that obtained from previous X-ray measurements of calmodulin (at similar concentrations) (Heidorn & Trewhella, 1988; Seaton et al., 1985). The maximum dimension, d_{max}, of the scattering particle is indicated to be approximately 66 Å (Table

Table III: Neutron Scattering Results for Calmodulin Complexed with PhK5 and PhK13

	P(*r*) analysis				Guinier analysis		
% D_2O	R_g (Å)	*I*(0) (cm)	χ^2	*n*[a]	R_g (Å)	*I*(0) (cm)	χ^2
0	31.5 ± 0.7	1.64 ± 0.08	1.4	4	29.1 ± 0.8	1.65 ± 0.09	1.0
20	26.3 ± 0.7	1.36 ± 0.08	0.8	4	23.7 ± 0.6	1.35 ± 0.07	0.6
40	25.9 ± 0.8	1.05 ± 0.06	1.3	4	24.3 ± 0.7	1.04 ± 0.06	0.8
100	9.8 ± 0.3	0.30 ± 0.06	1.1	2	9.5 ± 0.3	0.30 ± 0.06	1.1

[a] *n* is the number of sine terms in the *P*(*r*) series expansion (see Materials and Methods).

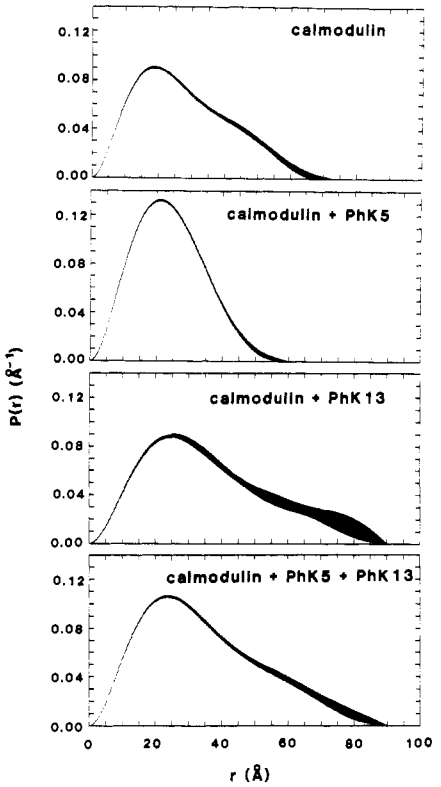

FIGURE 3: *P*(*r*) curves calculated from X-ray scattering data for calmodulin (13.3 mg/mL), calmodulin + PhK5 (18.3 mg/mL), calmodulin + PhK13 (6.7 mg/mL), and calmodulin + PhK5 + PhK13 (12.8 mg/mL). To facilitate comparisons, the areas under the *P*(*r*) curves have been normalized so that their ratios are equal to the respective ratios of the molecular weight for each complex. The band representing each *P*(*r*) curve is ±1 standard deviation in height, indicating propagated statistical errors.

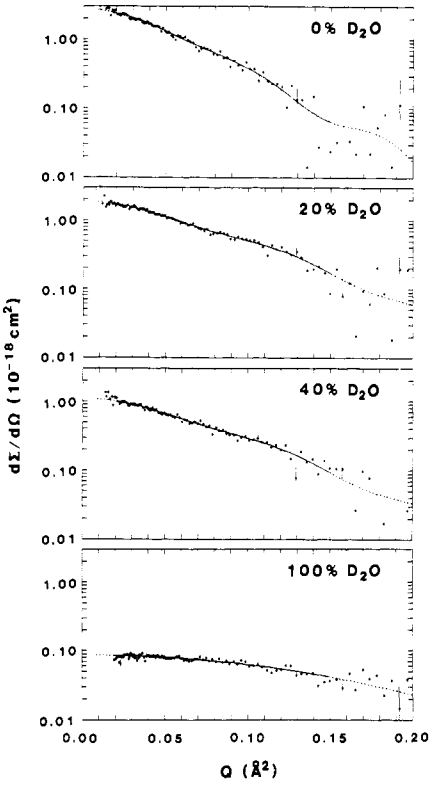

FIGURE 4: Neutron scattering data for partially deuterated calmodulin + PhK5 + PhK13 (24 mg/mL). Contrast between the scattering particle and the solvent was varied by changing the D_2O:H_2O ratio in the solvent; the percentages indicated represent the percentage of D_2O in the solvent. The neutron intensities are given as the differential scattering cross section ($d\Sigma(Q)/d\Omega$). The solid lines are the Fourier transforms of the *P*(*r*) model, and the dashed portions of the lines are extrapolations of the fits. Representative error bars based on counting statistics are shown.

II), and the *P*(*r*) has a maximum at approximately 18 Å with a shoulder at around 45 Å. This profile is consistent with a two-lobed structure (Heidorn & Trewhella, 1988). In contrast, the calmodulin + PhK5 *P*(*r*) curve indicates a dramatically reduced maximum dimension for the scattering particle (approximately 49 Å), and the *P*(*r*) curve is quite symmetric, with a single peak at approximately 21 Å. This indicates the complex is more compact and globular than calmodulin alone. The general contraction of the calmodulin + PhK5 particle compared with calmodulin is also reflected in the R_g value of 17.3 ± 0.19 Å, which is 15% smaller than that measured for calmodulin alone (Table II).

The structure of the calmodulin + PhK13 complex is quite different from that of calmodulin alone or the calmodulin + PhK5 complex (Figure 3; Table II). The calmodulin + PhK13 complex has a significantly larger R_g value than calmodulin (25.3 Å compared with 19.9 ± 0.19 Å) and a greater d_{max} (by about 20 Å). The *P*(*r*) curve for calmodulin + PhK13 is also markedly asymmetric. Its maximum is at approximately 25 Å with a slight shoulder at approximately 60 Å and a tail extending to long vector length values. The *P*(*r*) curve, and hence R_g and d_{max} values, for the calmodulin + PhK5 + PhK13 complex are not significantly different from those of the calmodulin + PhK13 complex, indicating similar solution structures for the two complexes.

Neutron Scattering. Data were collected from partially deuterated calmodulin complexed with equimolar amounts of nondeuterated PhK5 and PhK13 peptides. The solution conditions were identical with those used for the X-ray experiments. Neutron scattering data were measured at four different solvent contrasts by using 0%, 20%, 40%, and 100% D_2O (Figure 4). Table III summarizes the R_g, *I*(0), and reduced χ^2 values determined from the neutron scattering data. For a monodisperse solution of particles, a plot of the square root of the zero-angle scattering intensity versus the solvent scattering density (Figure 5) is expected to be linear with a slope equal to the volume of the scattering particle (Stuhrmann, 1976), assuming the intensity data are on an absolute scale. The LQD intensity scale has been calibrated by comparison of measurements of standard samples at a number of facilities (Hjelm & Seeger, 1989), including the well-calibrated Oak Ridge 30-m small-angle neutron spectrometer (Wignall & Bates, 1987). The slope from Figure 5 gives the volume of the scattering particle as 28 000 ± 1900 Å^3. The value for

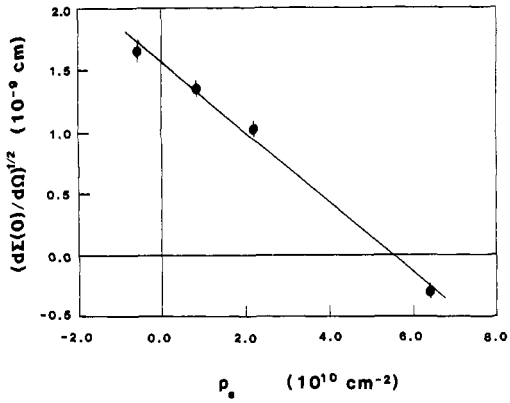

FIGURE 5: Dependence of the neutron forward scatter for partially deuterated calmodulin complexed with nondeuterated PhK5 and PhK13 on the solvent scattering density.

the particle volume determined from the neutron scattering data is in good agreement, within the statistical uncertainty, with the theoretical unhydrated particle volume (27 508 Å^3) calculated by using the known molecular weight of the particle (23 100) and assuming its specific volume to be 0.72 cm^3/g. The specific volume was simply estimated as the average of the range of values measured for most proteins (0.69–0.75 cm^3/g) since there are no experimental data available for this particular complex. [Klee and Vannaman (1982) have reported a value of 0.707 cm^3/g for 4Ca^{2+}–calmodulin alone.] The neutron data thus confirm there is no protein aggregation in the sample.

The intercept at zero intensity of the plot in Figure 5 gives the mean contrast match point for the particle, $\bar{\rho}$, as (5.5 ± 0.6) × 10^{10} cm^{-2}. The contrast match point is the mean scattering-length density of the particle (which depends on deuteration level and chemical composition) divided by the particle volume. Combined with the volume determined from the slope, the match point gives the deuteration level as 60%, which is reasonable given the growth conditions used for the bacteria that produced the deuterated calmodulin (approximately 75% deuterated medium). LeMaster and Richards (1988) found that thioredoxin isolated from an *Escherichia coli* bacterial expression system grown on 82–85% deuterated nutrients and 85% D_2O was deuterated at a level of 75%, reflecting the microorganisms' selective incorporation of hydrogen in preference to deuterium from the medium.

In 0% D_2O, both calmodulin and the peptides contribute to the neutron scattering, though the calmodulin contribution is larger since the contrast with respect to the solvent is higher for the deuterated calmodulin. For the X-ray measurements, both the peptides and calmodulin contribute equally to the scattering since they have the same mean electron density and hence the same X-ray scattering density. The 0% D_2O neutron data give a larger value for R_g than is obtained from the X-ray data for the calmodulin + PhK5 + PhK13 complex. Differences in R_g are expected due to differences in contrast and internal density fluctuations of the complex for X-rays and neutrons. As the contrast between the peptides and the solvent is reduced in the neutron contrast series (i.e., as the percentage of D_2O in the solvent is increased from 0% to 40%), and hence as their contribution to the scattering is decreased, the R_g values for the complex decrease (Table III). In 37–40% D_2O the mean neutron scattering density for the nondeuterated peptides is close to the scattering density of the solvent, based on the chemical composition and specific volume estimates for the peptides. The neutron scattering data from the complexes will therefore be dominated by the scattering from the deuterated calmodulin, although there will also be second-order effects caused by internal density fluctuations within the particle as well as any residual contribution from the peptides that may not be perfectly matched to the solvent. The R_g value obtained from the 40% D_2O data is significantly larger than any value obtained for calmodulin as a free monomer in solution by using X-ray scattering (Seaton et al., 1985; Heidorn & Trewhella, 1988; Table I) or neutron scattering (Heidorn et al., 1989), suggesting that calmodulin has a more extended structure when bound to PhK5 and PhK13. The simplest way to imagine a more extended conformation for calmodulin would be for the globular lobes to be moved apart. We have previously proposed that the interconnecting helix region of calmodulin in solution is flexible and the surfaces of the two globular lobes are, on average, closer together (by about 10 Å) compared with the crystal structure (Heidorn & Trewhella, 1988). Movement of the globular domains further apart induced, for example, by a stabilization of the interconnecting helix would result in increases in R_g and d_{max} values. However, without a more complete contrast variation study of this system it is not possible to model the calmodulin + PhK5 + PhK13 complex or its components in any more detail.

Ibel and Stuhrmann (1975) showed that the contrast dependence of R_g^2, for a scattering particle with two components of different mean scattering density, could be approximated by

$$R_g^2 = R_v^2 + (\alpha/\rho) + (\beta/\rho^2) \quad (1)$$

where R_v is the radius of gyration at infinite contrast, $\rho = \bar{\rho} - \rho_s$, $\bar{\rho}$ is the mean scattering density for the particle, and ρ_s is the solvent scattering density. The coefficient α is related to the second moment of the scattering density fluctuations about the mean value for the scattering particle, while β is related to the square of the first moment of the density fluctuations about the mean. Hence, α and β give information about the relative dispositions of the two scattering components. By fitting the R_g data to this function, one can, in theory, quantitatively determine the spatial relationship between the two components of the scattering particle. To facilitate an improved Stuhrmann analysis, the current experiments used calmodulin that was deuterated at a lower level than the calmodulin used in the earlier calmodulin + MLCK-I experiments. The objective was to measure data at both negative and positive contrast so that the parameters defining the parabola of eq 1 could be better determined than was possible in the previous experiment (for which only data at positive contrast were measured), thus quantifying the spatial relationship of calmodulin and the peptides in the complex more precisely. From Figure 5 it is evident; that we succeeded in measuring the calmodulin + PhK5 + PhK13 at both postive and negative contrast. Unfortunately, without prior knowledge of the contrast match point for the particle, it was difficult to determine the *optimal* level of deuteration for calmodulin; the single point that was measured at negative contrast was still to close too the contrast match point to determine the parameters of eq 1 precisely. We are therefore again confined to making a qualitative interpretation of the contrast dependence of the neutron scattering data. In the present case the data must be fitted by a parabola with a negative α and a nonzero β. The negative α and finite value for β is conclusive evidence that the center of mass of the peptides is more toward the outside of the complex compared with that of calmodulin.

Discussion

Work from a number of different laboratories has shown that peptides are useful tools for studying molecular aspects of calmodulin–target enzyme interactions. Previous studies

of calmodulin–peptide interactions have used peptides from a variety of sources, such as naturally occurring peptide hormones and venoms, as well as synthetic peptides with primary and secondary structures related to known target enzyme calmodulin-binding domains [reviewed in Blumenthal and Krebs (1988)]. The first target enzyme calmodulin-binding domain to be identified was that from rabbit skeletal muscle myosin light chain kinase (MLCK; Blumenthal et al., 1985). Synthetic peptides based on the sequence of this domain have been used in a number of studies to characterize calmodulin interactions that might be relevant to MLCK and other target enzymes. The MLCK peptides exhibit the propensity to form basic, amphipathic α-helices, a structural motif that appears to be found in a number of calmodulin-binding peptides that have been studied to date [reviewed by O'Neil and DeGrado (1990)]. When the present investigations were first undertaken, it was anticipated that there might be significant differences between the solution structures of calmodulin–peptide complexes containing γ-subunit peptides and complexes with the MLCK peptides and other peptides. These expectations were based on several previous observations regarding biochemical and structural differences between the γ-subunit and calmodulin target enzymes such as MLCK. MLCK and most other calmodulin-dependent enzymes bind calmodulin in a Ca^{2+}-dependent manner and rapidly dissociate when free Ca^{2+} concentrations are lowered to submicromolar levels. In contrast, the δ-subunit of phosphorylase kinase (calmodulin) remains tightly bound to the γ-subunit at submicromolar concentrations of Ca^{2+}, even in the presence of mild denaturants (Chan & Graves, 1982). Important structural differences between the calmodulin-binding domain of the γ-subunit and those of target enzymes such as MLCK also indicate that there may be significant differences between the respective calmodulin–peptide complexes. Whereas the calmodulin-binding domain of MLCK is contained within a single relatively short sequence (17 residues; Blumenthal & Krebs, 1987), the calmodulin-binding domain of the γ-subunit consists of two distinct noncontiguous subdomains (Dasgupta et al., 1989). Each of the γ-subunit subdomains is approximately the size of the MLCK calmodulin-binding domain (approximately 25 residues). Synthetic peptides based on the two γ-subunit subdomains are capable of simultaneously binding calmodulin, and both subdomain peptides can competitively inhibit binding of MLCK calmodulin-binding peptides (Dasgupta et al., 1989). These latter data indicate that neither of the γ-subunit peptides binds calmodulin in exactly the same way that the MLCK peptides do. The X-ray and neutron scattering data presented here provided additional evidence that the γ-subunit of phosphorylase kinase interacts with calmodulin in a manner fundamentally different from target enzymes like MLCK.

The structural parameters obtained previously from X-ray and neutron scattering experiments for the calmodulin + MLCK-I complex show there is a general contraction of calmodulin when MLCK-I is bound such that the two lobes of calmodulin are brought into close contact (Heidorn et al., 1989). Such a conformational change was proposed by O'Neil and DeGrado (1989) on the basis of photolabeling studies of calmodulin–peptide complexes, and a theoretical model for a calmodulin–MLCK peptide complex published by Persechini and Kretsinger (1988a) is in qualitative agreement with the scattering data. A similar pattern of structural changes observed for MLCK-I is observed in small-angle X-ray scattering studies of calmodulin complexed with the venom peptides melittin (Kataoka et al., 1989) and mastoparan (Matsushima et al., 1989; Yoshino et al., 1989). In the present study, the γ-subunit peptide, PhK5, is observed to cause structural changes in calmodulin that are comparable to changes induced by these other peptides as indicated by similar d_{max} values, R_g values, and $P(r)$ curves. The fact that PhK5 is predicted by Chou–Fasman analysis to form a structure that is largely a basic amphipathic helix (Dasgupta et al., 1989) similar to the predicted structures of MLCK-I, mastoparan, and melittin suggests that the ability of these peptides to induce similar structural changes in calmodulin is related to their propensity for folding into the basic amphipathic helix motif commonly found in calmodulin-binding peptides.

The structural parameters derived from the X-ray scattering data for the calmodulin + PhK13 peptide complex are strikingly different from those obtained for the calmodulin + PhK5 peptide complex or the calmodulin + MLCK-I peptide complex. The $P(r)$ curve is very asymmetric, and the R_g and d_{max} values for this complex are much larger than those obtained for the calmodulin–peptide complexes containing MLCK-I or PhK5 peptides. The R_g and d_{max} values are also significantly larger than calmodulin alone, indicating that PhK13 binds to calmodulin in such a way that its structure is extended somewhat and/or that the mass of the peptide extends beyond the periphery of the calmodulin component in the complex. There is no indication that Phk13 causes a contraction of calmodulin as is the case with the MLCK-I or PhK5 peptides. Secondary structure predictions of PhK13 indicate that the peptide is more likely to form a β-turn/β-sheet structure rather than an α-helix (Dasgupta et al., 1989). If these predictions are accurate, such as extended secondary structure for PhK13 might account for the extended type of structure observed for the peptide–calmodulin complexes containing PhK13 compared with the more compact structures observed with peptides predicted to form amphipathic α-helices.

When both PhK5 and PhK13 are bound to calmodulin, the $P(r)$ curve obtained from X-ray scattering closely resembles the $P(r)$ curve obtained with PhK13 alone. In addition, the R_g and d_{max} values for these two complexes are also nearly identical. These data indicate that when both γ-subunit peptides are bound to calmodulin, the effects of PhK13 predominate and the result is a complex that is highly extended when compared to calmodulin–peptide complexes containing MLCK-I or PhK5 alone. It is therefore reasonable to suggest that the δ-subunit of phosphorylase kinase (calmodulin) is bound to the γ-subunit in an extended conformation, rather than a contracted conformation as is thought to be the case for enzymes such as myosin light chain kinase. This extended conformation may be important for increasing intersubunit contacts required for optimal regulation of γ-subunit activity. Future studies will be directed toward determining whether the extended conformation of the δ-subunit exists in complexes containing larger γ-subunit peptides as well as complexes containing intact γ-subunit.

Previous neutron scattering data obtained at various solvent contrasts by using (deuterated) calmodulin + (nondeuterated) MLCK-I indicate that calmodulin forms a compact structure in the complex and the nondeuterated MLCK-I is located more toward the center of the complex, while the calmodulin is distributed more toward the outside of the complex. Neutron scattering data obtained in the present study at various solvent contrasts by using deuterated calmodulin and nondeuterated γ-subunit peptides indicate that calmodulin is in an extended conformation in this complex and that both peptides are not concentrated near the center of the complex. The Stuhrmann analysis indicates a significant proportion of the γ-subunit

peptides is distributed more toward the periphery of the complex. Due to experimental limitations (discussed under Results) it is not possible to extract higher resolution information regarding the localization of the γ-subunit peptides within the complex. Studies aimed at providing such information are currently in progress.

The characterization of the extended calmodulin–γ-peptide complexes provides further evidence that flexibility in the interconnecting helix plays an important role in facilitating different types of target enzyme interactions. On the basis of activation studies of a cross-linked mutant calmodulin, Persechini and Kretsinger (1988b) proposed the interconnecting helix region of calmodulin is a "flexible tether". Studies of mutant calmodulins in which residues have been deleted from the central helix region (Persechini et al., 1989; VanBerkum et al., 1990) show that activation of MLCK is relatively insensitive to shortening the helix by two, three, or four residues, consistent with the flexible tether hypothesis for MLCK activation. In contrast, phosphodiesterase activity is quite sensitive to deletions in the interconnecting helix, suggesting an extended conformation of calmodulin may be required for phosphodiesterase activity (VanBerkum et al., 1990). The X-ray and neutron scattering studies presented here suggest that the calmodulin–γ-subunit interaction may also require a certain minimum length in the interconnecting helix region.

It has been previously noted (Dasgupta et al., 1989) that there are sequence similarities between the calmodulin-binding subdomains of the γ-subunit of phosphorylase kinase and specific regions in the thin filament regulatory protein troponin I (TnI). In particular, the TnI sequence 104–115 known to be important in binding TnC and actin (Syska et al., 1976; Leszyk et al., 1987; Van Eyk & Hodges, 1988) has a five-residue sequence that is identical with part of the PhK13 sequence. CD studies of TnC and calmodulin with the TnI-(104–115) peptide and with the wasp venom mastoparan show a dramatic increase in helix content when mastoparan is complexed with either calmodulin or TnC, whereas there is no change in helical content when either protein binds the TnI(104–115) peptide (Cachia et al., 1986). These data suggest that TnC and calmodulin may undergo similar structural changes upon binding peptides with similar sequences. Hence, one might expect that TnC, which is structurally homologous to calmodulin, also has an extended structure when bound to TnI.

Acknowledgments

We thank James Rokop for technical assistance in the reduction and analysis of the X-ray scattering data. We also thank Anthony Means for making available the bacterial expression system that was used to produce the deuterated calmodulin and Henry Crespi for the deuterated algae that were used as a source of deuterated nutrients.

References

Babu, Y. S., Sack, J. S., Greenhough, T. C., Bugg, C. E., Means, A. R., & Cook, W. J. (1985) *Nature 315*, 37.

Babu, Y. S., Bugg, C. E., & Cook, W. J. (1988) *J. Mol. Biol. 204*, 191.

Bayley, P., Martin, S., & Jones, G. (1988) *FEBS Lett. 238*, 61.

Blumenthal, D. K., & Krebs, E. G. (1987) *Methods Enzymol. 139*, 115.

Blumenthal, D. K., & Krebs, E. G. (1988) in *Molecular Aspects of Cellular Regulation* (Cohen, P., Klee, C. B., Eds.) Vol. 5, pp 341–356, Elsevier, Amsterdam.

Blumenthal, D. K., Takio, K., Edelman, A. M., Charbonneau, H., Titani, K., Walsh, K. A., & Krebs, E. G. (1985) *Proc. Natl. Acad. Sci. U.S.A. 82*, 3187.

Cachia, P. J., Van Eyk, J., Ingraham, R. H., McUbbin, W. D., Kay, C. M., & Hodges, R. S. (1986) *Biochemistry 25*, 3553.

Chan, K.-F. J., & Graves, D. J. (1982) *J. Biol. Chem. 257*, 5956.

Dasgupta, M., Honeycutt, T., & Blumenthal, D. K. (1989) *J. Biol. Chem. 264*, 8054.

Fasman, G., Ed. (1989) *CRC Practical Handbook of Biochemistry and Molecular Biology*, pp 81–82, CRC Press, Boca Raton, FL.

Guinier, A. (1939) *Ann. Phys. (Paris) 12*, 161.

Heidorn, D. B., & Trewhella, J. (1988) *Biochemistry 27*, 909.

Heidorn, D. B., Seeger, P. A., Rokop, S. E., Blumenthal, D. K., Means, A. R., Crespi, H., & Trewhella, J. (1989) *Biochemistry 28*, 6757.

Hjelm, R. P., & Seeger, P. A. (1989) in *Advanced Neutron Sources: Proceedings of the 10th Meeting of the International Collaboration on Advanced Neutron Sources (ICANS X)*, Los Alamos, Oct 1988, p 367.

Ibel, K., & Stuhrmann, H. B. (1975) *J. Mol. Biol. 93*, 255.

Kataoka, M., Head, J. F., Seaton, B. A., & Engelman, D. M. (1989) *Proc. Natl. Acad. Sci. U.S.A. 86*, 6944.

Klee, C. B., & Vannaman, T. C. (1982) *Adv. Protein Chem. 35*, 213.

Kringbaum, W. R., & Kugler, F. R. (1970) *Biochemistry 9*, 1216.

LeMaster, D., & Richards, F. (1988) *Biochemistry 27*, 142.

Leszyk, J., Collins, J. H., Leavis, P. C., & Tao, T. (1987) *Biochemistry 26*, 7042.

Matsushima, N., Izumi, Y., Matsuo, T., Yoshino, Y., Ueki, T., & Miyake, Y. (1989) *J. Biochem. (Tokyo) 105*, 883.

Moore, P. B. (1980) *J. Appl. Crystallogr. 13*, 168.

O'Neil, K. T., & DeGrado, W. F. (1990) *Trends Biochem. Sci. 15*, 59.

O'Neil, K. T., Erickson-Viitanen, S., & Degrado, W. F. (1989) *J. Biol. Chem. 264*, 14571.

Persechini, A., & Kretsinger, R. H. (1988a) *J. Cardiovasc. Pharmacol. 12* (Suppl. 5), S1.

Persechini, A., & Kretsinger, R. H. (1988b) *J. Biol. Chem. 263*, 12175.

Persechini, A., Blumenthal, D. K., Jarrett, H. W., Klee, C. B., O'Hardy, D. O., & Kretsinger, R. H. (1989) *J. Biol. Chem. 264*, 8052.

Pickett-Giess, C. A., & Walsh, D. A. (1986) *Enzymes (3rd Ed.) 17*, 396–459.

Picton, C., Klee, C. B., & Cohen, P. (1980) *Eur. J. Biochem. 111*, 553.

Porod, G. (1951) *Kolloid Z. 124*, 83.

Seaton, B. A., Head, J. F., Engelman, D. M., & Richards, F. M. (1985) *Biochemistry 24*, 6740.

Seeger, P. A., Williams, A., & Trewhella, J. (1987) in *Proceedings of the 9th International Collaboration on Advanced Neutron Sources* (Atchison, F., & Fischer, W., Eds.) SIN Report ISBN 3-907990-01-4, p 437, Swiss Institute for Nuclear Research, Villigen, Switzerland.

Seeger, P. A., Hjelm, R. P., & Nutter, M. J. (1990) *Mol. Cryst. Liq. Cryst. 108A*, 101.

Stuhrmann, H. B. (1976) *Brookhaven Symp. Biol. 27*, IV-3–IV-19.

Syska, H., Wilkinson, J. M., Grand, R. J. A., & Perry, S. V. (1976) *Biochem. J. 153*, 375.

VanBerkum, M. F. A., George, S. E., & Means, A. R. (1990)

J. Biol. Chem. 265, 3750.
Van Eyk, J. E., & Hodges, R. S. (1988) J. Biol. Chem. 263, 1726.
Watterson, D. M., Harrelson, W. G., Jr., Keller, P. M., Sarif, F., & Vannaman, T. C. (1976) J. Biol. Chem. 251, 4501.
Wignall, G. D., & Bates, F. S. (1987) J. Appl. Crystallogr. 20, 28.
Wu, C.-F., & Chen, S.-H. (1988) Biopolymers 27, 1065.
Yoshino, H., Minari, O., Matsushima, N., Ueki, T., Miyake, Y., Matsuo, T., & Izumi, Y. (1989) J. Biol. Chem. 264, 19706.
Zaccai, G., & Jacrot, B. (1983) Annu. Rev. Biophys. 12, 139.

High-Resolution Three-Dimensional Structure of a Single Zinc Finger from a Human Enhancer Binding Protein in Solution†

James G. Omichinski,‡ G. Marius Clore,*,‡ Ettore Appella,§ Kazuyasu Sakaguchi,§ and Angela M. Gronenborn*,‡

Laboratory of Chemical Physics, Building 2, National Institute of Diabetes and Digestive and Kidney Diseases, and Laboratory of Cell Biology, Building 37, National Cancer Institute, National Institutes of Health, Bethesda, Maryland 20892

Received May 8, 1990; Revised Manuscript Received July 3, 1990

ABSTRACT: The three-dimensional structure of a 30-residue synthetic peptide containing the carboxy-terminal "zinc finger" motif of a human enhancer binding protein has been determined by two-dimensional nuclear magnetic resonance (2D NMR) spectroscopy and hybrid distance geometry–dynamical simulated annealing calculations. The structure determination is based on 487 approximate interproton distance and 63 torsion angle (ϕ, ψ, and χ_1) restraints. A total of 40 simulated annealing structures were calculated, and the atomic rms distribution about the mean coordinate positions (excluding residues 29 and 30 which are ill-defined) is 0.4 Å for the backbone atoms, 0.8 Å for all atoms, and 0.41 Å for all atoms excluding the lysine and arginine side chains, which are disordered. The solution structure of the zinc finger consists of two irregular antiparallel β-strands connected by an atypical turn (residues 3–12) and a classical α-helix (residues 14–24). The zinc is tetrahedrally coordinated to the sulfur atoms of two cysteines (Cys-5 and Cys-8) and to the $N^{\epsilon 2}$ atoms of two histidines (His-21 and His-27). The two cysteine residues are located in the turn connecting the two β-strands (residues 5–8); one of the histidine ligands (His-21) is in the α-helix, while the second histidine (His-27) is at the end of a looplike structure (formed by the end of the α-helix and a turn). The general architecture is qualitatively similar to two previously determined low-resolution Cys_2His_2 zinc finger structures, although distinct differences can be observed in the β-strands and turn and in the region around the two histidines coordinated to zinc. Comparison of the overall polypeptide fold of the enhancer binding protein zinc finger with known structures in the crystallographic data base reveals a striking similarity to one region (residues 23–44) of the X-ray structure of proteinase inhibitor domain III of Japanese quail ovomucoid [Papamokos, E., Weber, E., Bode, W., Huber, R., Empie, M. W., Kato, I., & Laskowski, M. (1982) J. Mol. Biol. 158, 515–537], which could be superimposed with a backbone atomic rms difference of 0.95 Å on residues 3–25 (excluding residue 6) of the zinc finger from the enhancer binding protein. The presence of structural homology between two proteins of very different function may indicate that the so-called zinc finger motif is not unique for a class of DNA binding proteins but may represent a general folding motif found in a variety of proteins irrespective of their function.

Recently, a number of cDNA clones coding for specific DNA binding proteins that interact with a variety of different enhancer and promotor regions of human genes have been isolated. The respective proteins have been designated human immunodeficiency virus type I enhancer binding protein (HIV-EPI;[1] Maekawa et al., 1989), major histocompatibility complex binding protein 1 (MBP-1; Singh et al., 1988), and positive regulatory domain II of the human interferon β promotor binding factor 1 (PRDII-BF1; Fan & Maniatis, 1990). HIV-EP1 was identified as a DNA binding protein that interacts with a specific DNA sequence within the long terminal repeats of the HIV-I genome, functioning as an enhancer element in HIV transcriptional regulation (Maekawa et al., 1989). MBP-1 was shown to bind specifically to the promotor of the MHC class I H-$2K^b$ gene and to a similar site within the immunoglobulin κ gene (Singh et al., 1988), and PDRII-BF1 binds to PDRII, a virus-inducible element

† This work was supported by the Intramural AIDS Targeted Antiviral Program of the Office of the Director of the National Institutes of Health (G.M.C. and A.M.G.).

* Authors to whom correspondence should be addressed.
‡ Laboratory of Chemical Physics, NIDDK.
§ Laboratory of Cell Biology, NCI.

[1] Abbreviations: HIV-EP1, human immunodeficiency virus type I enhancer binding protein; HIV-1, human immunodeficiency virus type I; PRDII, positive regulatory domain II of the human interferon β promotor; PRDII-BF1, positive regulatory domain II of the human interferon β promotor binding factor 1; MHC, major histocompatibility complex; MBP-1, major histocompatibility complex binding protein 1; NOE, nuclear Overhauser effect; NOESY, two-dimensional nuclear Overhauser enhancement spectroscopy; PE-COSY, primitive exclusive two-dimensional correlated spectroscopy; HOHAHA, two-dimensional homonuclear Hartmann–Hahn spectroscopy; SA, simulated annealing; HPLC, high-performance liquid chromatography; rms, root mean square.